Hindawi Publishing Corporation
International Journal of Antennas and Propagation
Volume 2016, Article ID 9280234, 10 pages
http://dx.doi.org/10.1155/2016/9280234

Research Article

A SIW Antipodal Vivaldi Array Antenna Design

Ying Suo,[1,2] Wei Li,[1] and Jianzhong Chen[1]

[1]*School of Electronics and Information Engineering, Harbin Institute of Technology, Harbin 150001, China*
[2]*Electronic Science and Technology Postdoctoral Station, Harbin Institute of Technology, Harbin 150001, China*

Correspondence should be addressed to Ying Suo; suoyingsing@126.com

Received 5 November 2015; Revised 25 December 2015; Accepted 28 December 2015

Academic Editor: Wei Liu

A kind of compact SIW (substrate integrated waveguide) Vivaldi array antenna is proposed and analyzed. The antenna consisted of 4 Vivaldi structure radiation elements fed by an equal power divider with SIW technology. The radiation element is composed of antipodal index gradient microstrip lines on both sides of the substrate. The measured reflection coefficient of the array antenna is less than −10 dB from 8.88 GHz to 10.02 GHz. The measured gain of the array antenna is 13.3 dB on 9.5 GHz.

1. Introduction

The Vivaldi antenna has been used in many microwave engineering applications for its simple structure, low cross polarization, and highly directive patterns characteristics, especially in ultra bandwidth applications such as vehicular wireless communication, radar imaging, and through-the-wall imaging [1–3]. Many kinds of Vivaldi antennas have been investigated for wideband application [4, 5], and some new antipodal Vivaldi antennas have been designed to improve radiation pattern and directivity [6, 7].

An equal power divider is necessary for the antenna array feed network for equal amplitude design. The SIW multiway microwave power divider attracts a lot of attentions because of its advantages such as small structural dimension, high integration, and low cost [8–10]. A Vivaldi antenna array fed by a SIW printed on a thick substrate is proposed in [11]. A compact four-element printed Vivaldi array is designed and investigated in [12].

The SIW is able to be fabricated by standard low cost PCB technique using low loss and low cost material substrates [13]. There is often a higher return loss in an array antenna system than a single antenna one as the feeding network for an array antenna, such as T-junction or Y-junction waveguide, will introduce a discontinuity where reflection increases sharply. To reduce the return loss, many approaches have been proposed. Reference [14] focused on the structure of its linear tapered array antennas, compared the reflection coefficients of three different structures of the array antenna, and found a maximum −10 dB bandwidth of 0.8 GHz in X-band, though the bandwidth is not wide.

To broaden the bandwidth of the array antenna, a Vivaldi array antenna operating in X-band is designed and measured in this paper. Return loss is optimized in both antenna and feed network. Vivaldi antenna is used as the array antenna element for enlarging the bandwidth. To reduce the return loss, metal via-holes are added and adjusted in the SIW. The antenna consisted of 4 Vivaldi antenna elements fed by a SIW equal power divider. Each Vivaldi element is composed of antipodal index gradient microstrip lines on both sides of the substrate, and SIW-microstrip transition structure is designed for measurement and connection. Finally this paper achieved an antenna design operating in X-band.

2. 4-Way SIW Power Divider Design

A SIW is composed of two columns of cylinder metal via-holes in the side faces of a dielectric substrate and metal layers on the upper and lower faces. The transmission characteristics of a SIW are almost the same as those of its equivalent metal waveguide. As SIWs are often integrated with coplanar waveguides or microstrip lines, transition structures should be designed for the connection. The transition structure must have a low insertion loss, a wide working band, and a simple geometry to be fabricated. The SIW connected with the microstrip transition is shown in Figure 1.

Table 1: Parameters of the 4-way SIW power divider.

Parameters (mm)																				
a	p	D_0	h_1	h_2	h_3	Z_1	Z_2	D_1	D_2	D_3	D_4	t_1	w_2	t_2	t_3	w_4	t_4	W	D	H
12	1	0.6	4	17	17	1.6	0.2	0.5	0.5	0.6	0.3	4.9	5.5	5	5	5	7	2	3.2	4.5

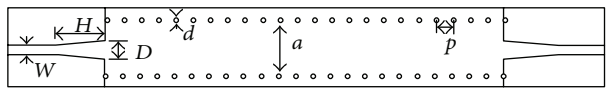

Figure 1: SIW with the microstrip transition.

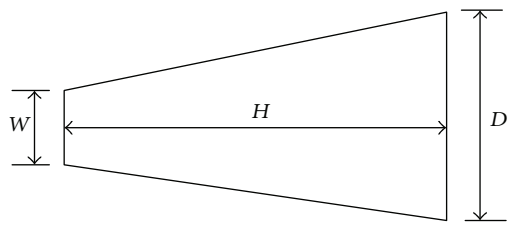

Figure 2: Tapered microstrip line.

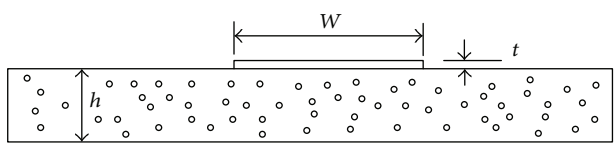

Figure 3: Microstrip line profile.

In Figure 1, a is the distance between the two columns of cylinder metal via-holes in the SIW, p is the distance between via-holes in the via-holes array. Since the field of the microstrip line is similar to the TE10 mode of the substrate integrated waveguide, the SIW-microstrip transition is generally a tapered microstrip line. The tapered line shown in Figure 2 is able to realize impedance transformation between the 50 Ω microstrip line and the substrate integrated waveguide.

As the tapered line is designed to realize impedance transformation, the left width of the tapered line W should equal the width of the 50 Ω microstrip line. The right width of the tapered line D should ensure that the impedance of the microstrip line equals that of the SIW.

For the microstrip line, as is shown in Figure 3, its width is W; thickness is t; when the thickness of the dielectric is h, the relative permittivity is ε_r.

The impedance of the microstrip line will be

$$Z_0 = \frac{60}{\sqrt{\varepsilon_{re}}} \ln\left(\frac{8h}{W} + \frac{W}{4h}\right) (\Omega) \quad W \le h,$$
$$Z_0 = \frac{120\pi}{\sqrt{\varepsilon_{re}}\,[W/h + 1.393 + 0.667 \ln(W/h + 1.444)]} (\Omega) \quad W \ge h, \tag{1}$$

where

$$\varepsilon_{re} = \frac{\varepsilon_r + 1}{2} + \frac{\varepsilon_r - 1}{2}\left[\left(2 + \frac{12h}{W}\right)^{-1/2} + 0.041\left(1 - \frac{W}{h}\right)^2\right] \quad W \le h,$$
$$\varepsilon_{re} = \frac{\varepsilon_r + 1}{2} + \frac{\varepsilon_r - 1}{2}\left(1 + 12\frac{h}{W}\right)^{-1/2} \quad W \ge h. \tag{2}$$

The equivalent impedance of the SIW in its TE mode is

$$Z_{\mathrm{TE10}} = \frac{\eta}{\sqrt{1 - (\lambda/2a)}}. \tag{3}$$

Ordinary Y-shaped structure can achieve the power division, but its discontinuous geometry will result in high return loss in pass band. Figure 4 shows that a 4-way SIW equal power divider is designed. The parameters of the four-way SIW power splitter are shown in Table 1. As is shown in Figure 4, adding a metal via-hole in the 90-degree bend of the SIW can reduce the power reflection when the electric field distribution of the Y-junction is changed by surface current distribution of the metal via-hole inductance. By adjusting the diameter and position of the via-hole, the least reflection can be obtained after simulation.

For parameters in Figure 4, D_0 is the diameter of the via-holes, h_1 is the width of the connection structure, h_2 is the width of the first section of Y-junction structure, h_3 is the width of the second Y-junction structure, Z_1 is the thickness of the dielectric slab, and Z_2 is the thickness of PEC in the simulation setting. It can be seen that D_1, D_2, D_3, and D_4 are the diameters of the inductive via-hole while t_1, t_2, t_3, t_4, w_2,

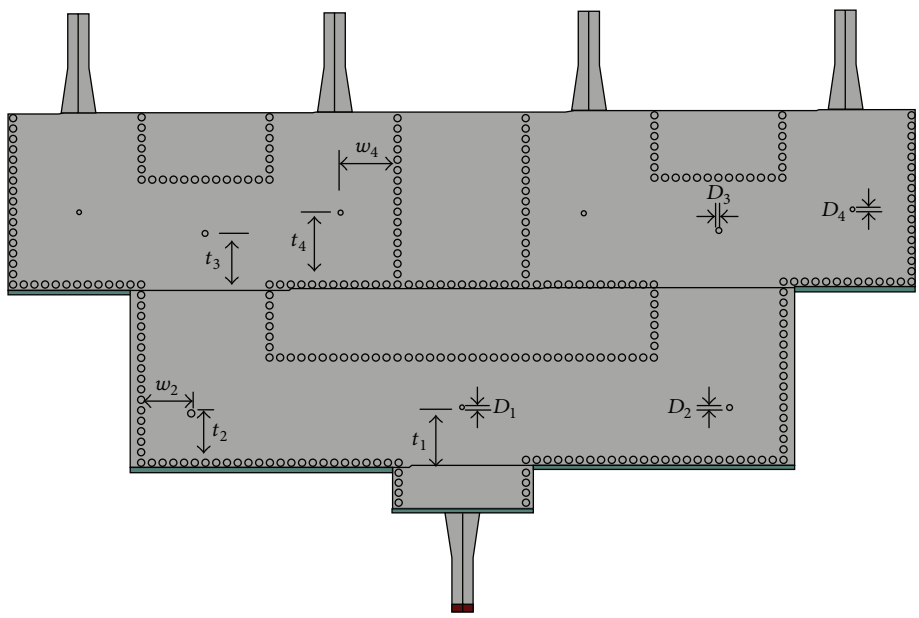

Figure 4: 4-way SIW power divider.

and w_4 determine the position of the via-holes. One via-hole is on the perpendicular bisector of the entire structure and the other two via-holes are on the perpendicular bisectors of the two upper Y-junctions, so there are no parameters w_1 and w_3.

To be tested by coaxial cable, five SIW microstrip transitions are connected with the SIW power splitter. The parameters of the microstrip transitions mentioned above are W, D, and H. W equals 2 and D equals 3.2, which ensures the impedance transformation of the 50 Ω microstrip line and the SIW. L is optimized to 4.5 for the least reflection loss.

After all the via-holes get their optimized diameter and position that are shown in Table 1, the 4-way SIW power divider is simulated. The permittivity of the substrate is 4.3, and the loss tangent is 0.0015 as used in this design. The simulated S-parameters of different ports are shown in Figure 5. It can be seen that the S_{11} parameter is less than −10 dB from 8.5 GHz to 10.5 GHz. In Figure 5, the transmission coefficient of S_{21}, S_{31}, S_{41}, and S_{51} is the same for the equal power division. As shown in Figure 5, the transmission coefficient of the power divider is −6.3 dB~−6.6 dB from 8.9 GHz to 10.07 GHz, so it is suitable for the 4-element antenna array design, and the insertion loss is about 0.3~0.6 dB from 8.9 GHz to 10.07 GHz.

The simulated surface current of the SIW divider on 9.5 GHz is shown in Figure 6. And the simulated electric field of the SIW divider on 9.5 GHz is shown in Figure 7.

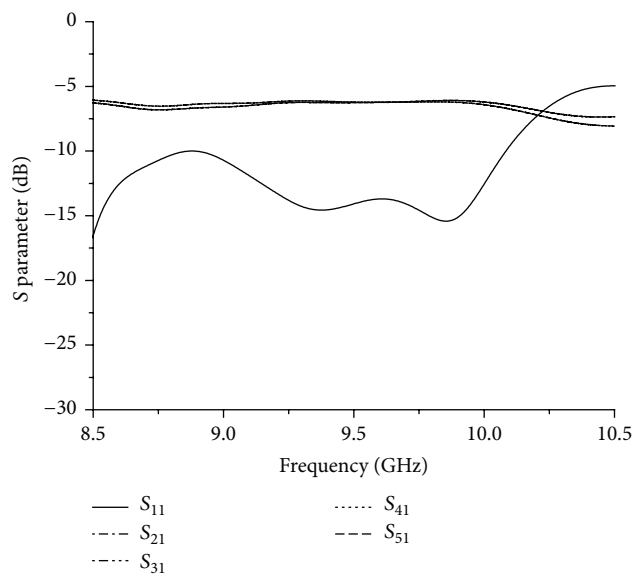

Figure 5: S parameters of the 4-way SIW power divider.

3. Antipodal Vivaldi Antenna Array Design

The antipodal Vivaldi radiation element is composed of complementary structures on both sides of the substrate. The antenna element is shown in Figure 8. The upper part is the antenna radiator, the middle part is the connection structure, and the lower part is the microstrip transition. For the upper radiation part of the antenna shown in Figure 8(a), the radiator is bordered by part of an ellipse curve on the right and an index gradient curve on the left. The index gradient curve whose exponential rate r equals 1 satisfies the following formula:

$$y = c_1 \times e^{rz} + c_2. \tag{4}$$

The Vivaldi antenna is directly fed by a microstrip line. Impedance of the microstrip is equal to that of each export of the equal power divider. A SIW-microstrip transition

Table 2: Parameters of the Vivaldi antenna element.

Parameters (mm)						
w_1	R	L	L_1	L_2	L_3	w_s
8.35	6.2	30.37	8.2	17	12.67	11.4

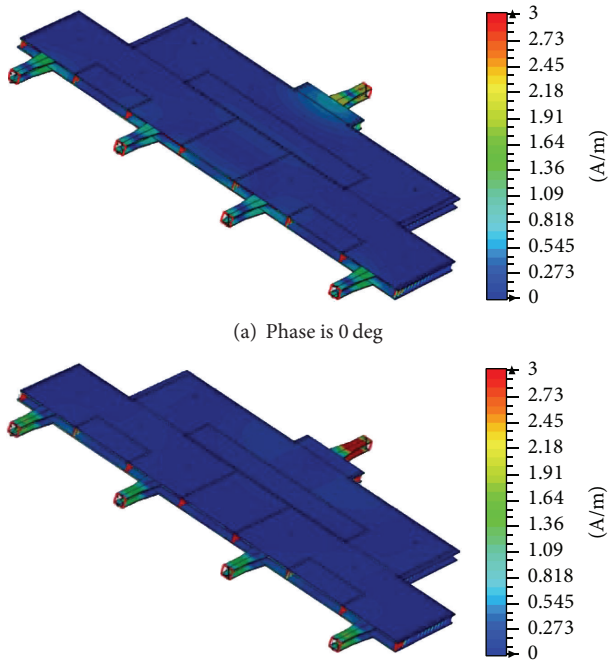

(a) Phase is 0 deg

(b) Phase is 90 deg

Figure 6: Surface current of the 4-way SIW power divider.

structure is designed for measurement and connection. The transition section is a tapered microstrip line.

As is shown in Figure 8, w_s is the antenna width, L is the antenna length, L_2 is set for the length of straight part in SIW-microstrip transition, L_1 is the length of the connection part, and L_3 is the length of the radiator. R is length of the truncated elliptic curve. The parameters of the Vivaldi radiation element are shown in Table 2.

Parameters on Table 2 are also optimized to get the best radiation characteristics of the antenna. The simulation model of antipodal Vivaldi antenna based on 4-way SIW power divider is shown in Figure 9. The dielectric substrate has a relative permittivity of 4.5 and a thickness of 1.6 mm. Parameters of the antenna and the SIW equal power divider equal those in Tables 1 and 2.

To get the optimized parameters of the diameter and position of a via-hole, S_{11} of the 4-way SIW power divider is simulated when one of the parameters of the via-hole varies. Because of the symmetry of the SIW, 4 of the 9 via-holes need to be analyzed.

Figure 10 shows the simulated S_{11} when the diameter of via-hole 1 D_1 varies from 0.3 to 0.6. It can be seen that the S_{11} curve moves up when D_1 increase, but not very much. Then 0.5 is picked as the optimized value of D_1 based on the S_{11} curves.

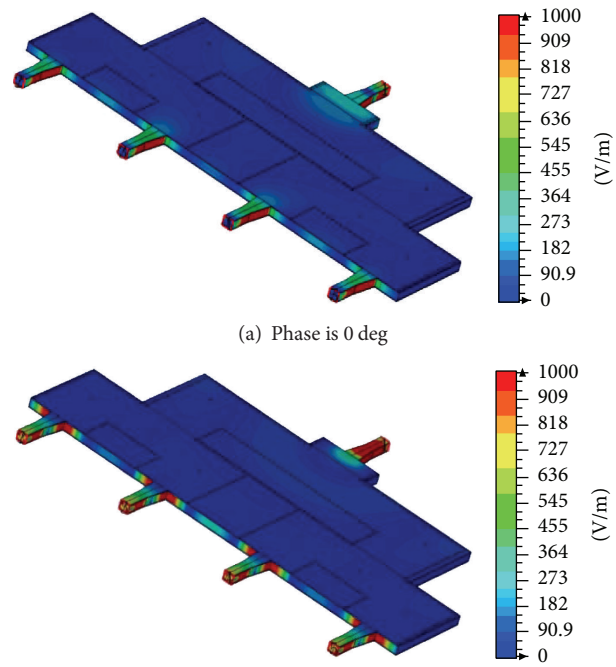

(a) Phase is 0 deg

(b) Phase is 90 deg

Figure 7: Electric field of the 4-way SIW power divider.

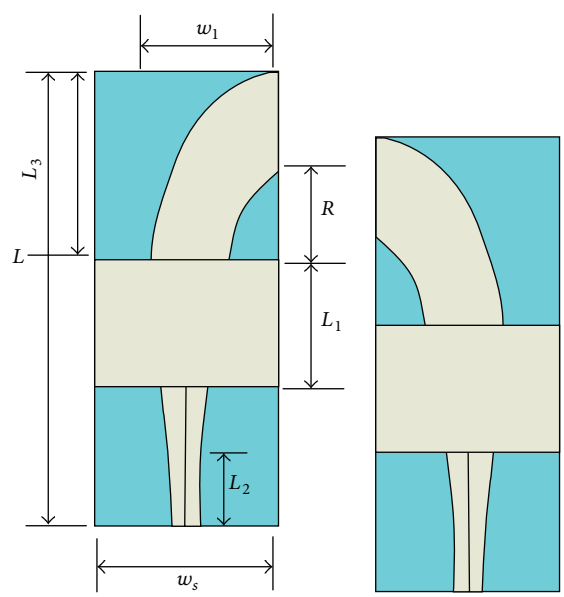

(a) Upper part (b) Lower part

Figure 8: Antipodal Vivaldi antenna element.

S_{11} when t_1 varies from 3 to 6 is shown in Figure 11. In Figure 11, the S_{11} curve firstly moves down and then moves up as t_1 increases. Therefore the optimized t_1 lies between 4 and 5. Obviously S_{11} is vastly dependent on t_1, so repeated simulations were carried out for the least reflection, which have ultimately shown that 4.9 is the best t_1 value.

Figure 12 has shown the simulated S_{11} curves when the diameter of via-hole 2 D_2 varies from 0.2 to 0.6. The S_{11} is

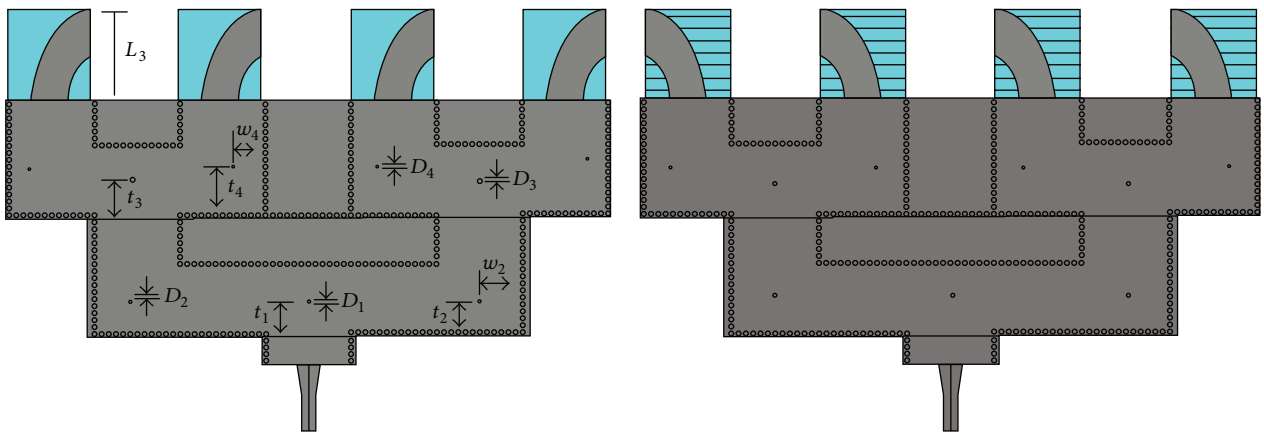

(a) Upper part (b) Lower part

Figure 9: Simulation model of the SIW Vivaldi antenna array.

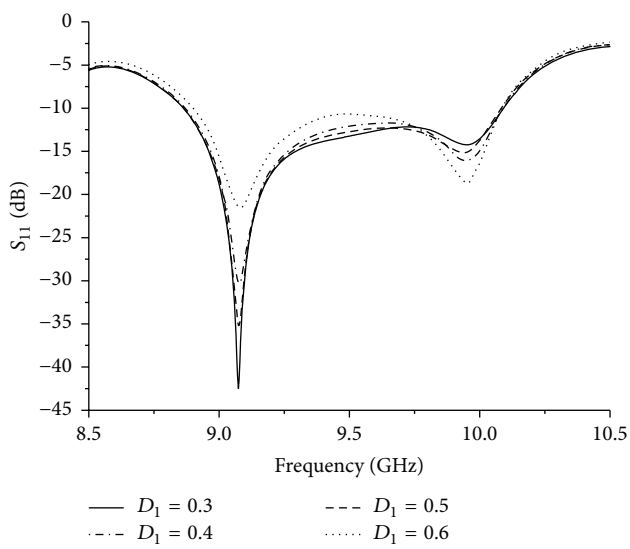

Figure 10: S_{11} when D_1 varies.

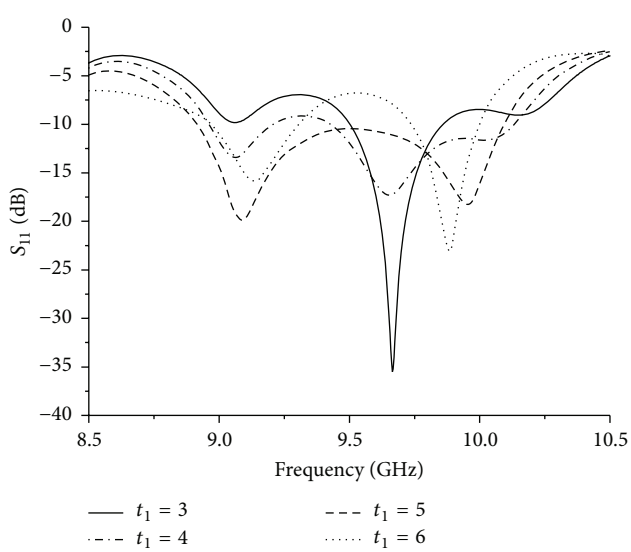

Figure 11: S_{11} when t_1 varies.

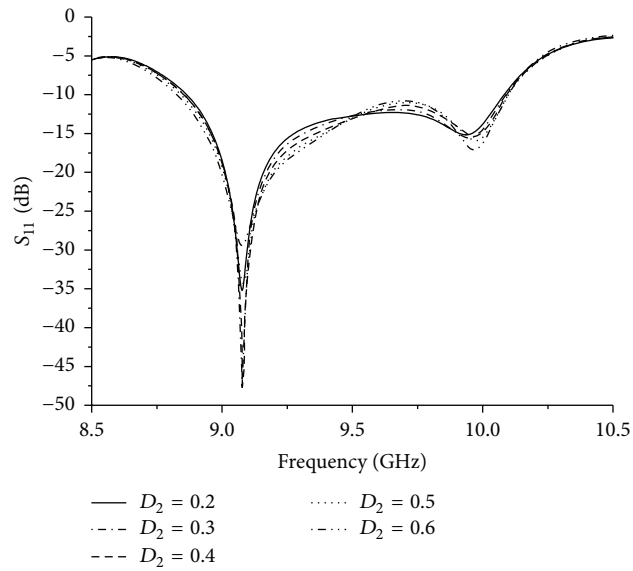

Figure 12: S_{11} when D_2 varies.

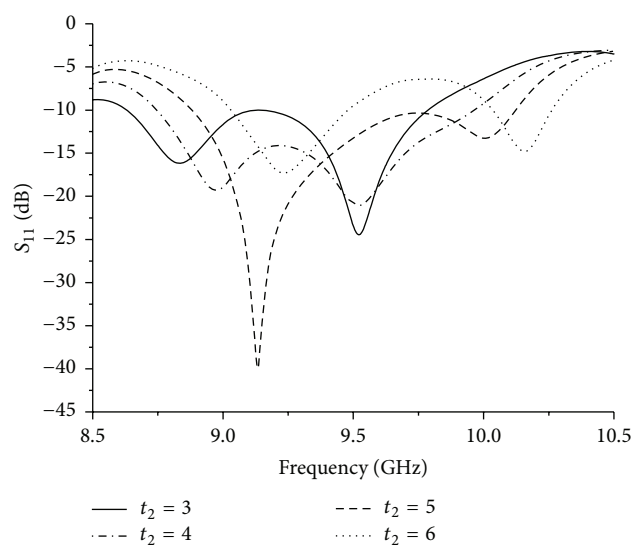

Figure 13: S_{11} when t_2 varies.

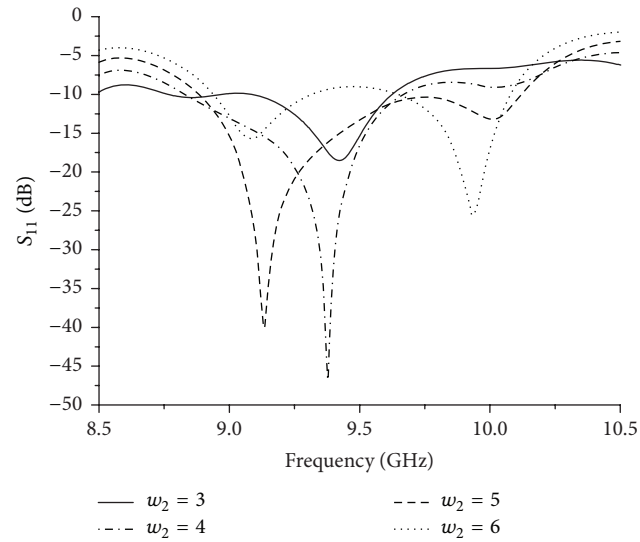

Figure 14: S_{11} when w_2 varies.

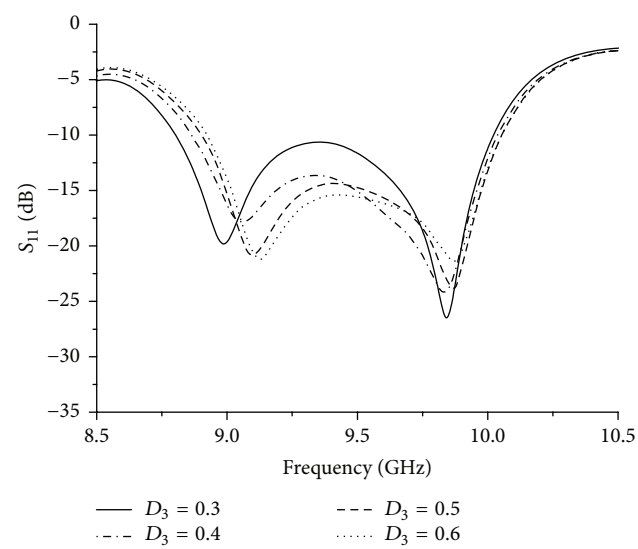

Figure 15: S_{11} when D_3 varies.

also not very dependent on D_2. For both low reflection loss and wide bandwidth, 0.5 is picked as D_2.

S_{11} when t_2 varies from 3 to 6 is shown in Figure 13. When t_2 increases, the S_{11} curve firstly moves down and then moves up, but the two resonate frequencies of the S_{11} curve moves right continuously. In consideration of both bandwidth and center frequency, $t_2 = 5$ is chosen.

Simulated S_{11} is shown in Figure 14 when w_2 varies from 3 to 6. As w_2 increases, the two center frequencies are moving left. The optimized w_2 lies between 4 and 6. After repeated simulation, 5.5 is found to be the optimized w_2.

S_{11} when D_3 varies from 0.3 to 0.6 is shown in Figure 15. The S_{11} curve is much more dependent on D_3 than D_1 and D_2, which moves down as D_3 increases. 0.5 is picked as the optimized D_3.

S_{11} when t_3 varies from 3 to 6 is shown in Figure 16. The S_{11} curve firstly moves down and then moves up, but the two center frequencies keep moving right, as t_3 increases. 4 is picked as the value of t_3.

Figure 17 shows the S_{11} curves of the SIW when the diameter of via-hole 4 varies from 0.3 to 0.6. The high frequency part of the S_{11} curve moves up while the low frequency part moves down as D_4 increases. So 0.3 is picked as the optimized D_4 for wider bandwidth.

S_{11} when t_4 varies is shown in Figure 18. The S_{11} curve firstly moves down and then moves up as t_4 increases. The optimized t_4 lies between 7 and 8. Later simulations have found that 7 is the optimized t_4.

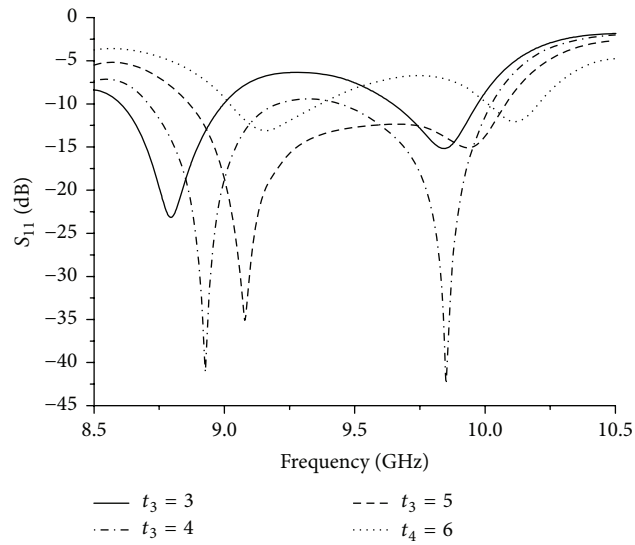

Figure 16: S_{11} when t_3 varies.

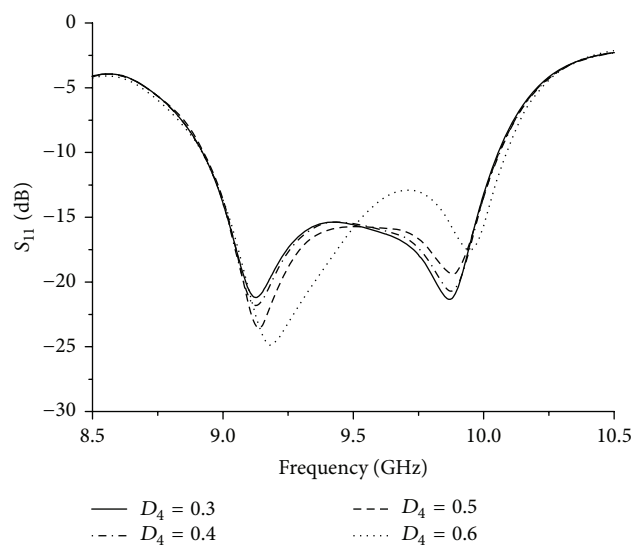

Figure 17: S_{11} when D_4 varies.

S_{11} when w_4 varies from 3 to 6 is simulated and shown in Figure 19. The bandwidth of the curves changes a little while the center frequencies change more when w_4 increases. So 4 is picked as the value of w_4 in consideration of the two center frequencies.

As is shown in Figure 20, a 4-element antipodal SIW Vivaldi antenna array is fabricated and measured. The total dimension of the antenna array is 85 mm × 7 mm with the feeding cable head. The parameters of the antenna array are $D_1 = 0.5$ mm, $t_1 = 4.9$ mm, $D_2 = 0.5$ mm, $t_2 = 5$ mm, $w_2 = 5.5$ mm, $D_3 = 0.5$ mm, $t_3 = 4$ mm, $D_4 = 0.3$ mm, and $t_4 = 4$ mm.

Figure 21 shows the simulated and measured reflection coefficient. Simulated results show that the reflection coefficient is less than −10 dB from 8.9 GHz to 10.07 GHz. And the measured reflection coefficient is less than −10 dB from

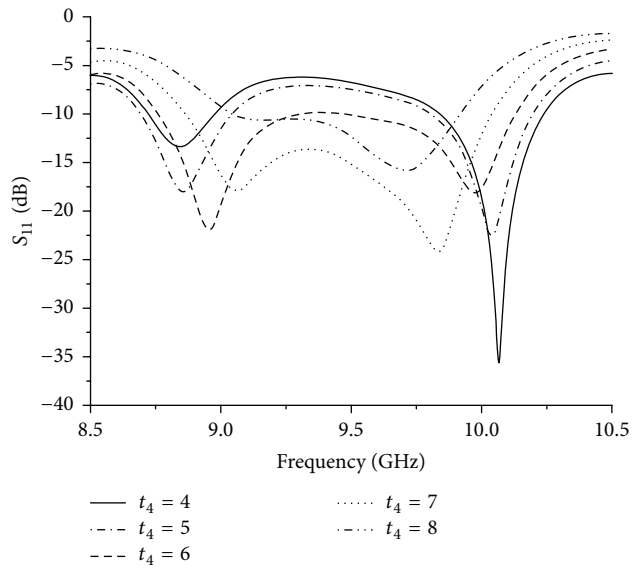

Figure 18: S_{11} when t_4 varies.

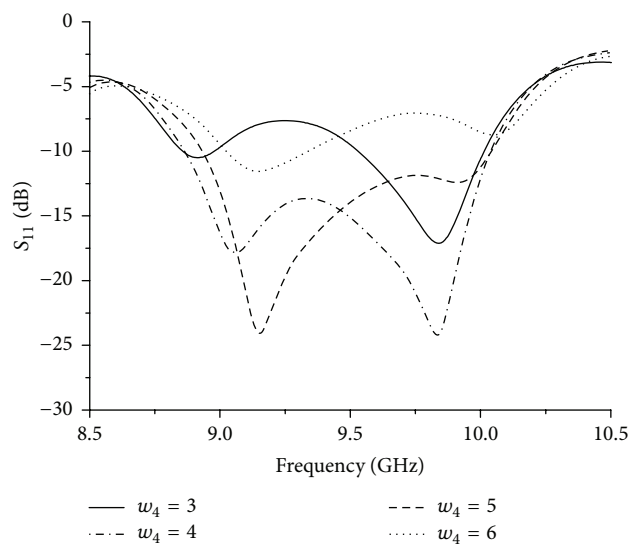

Figure 19: S_{11} when w_4 varies.

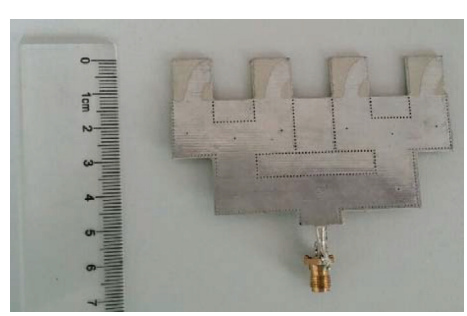

Figure 20: Fabricated antipodal SIW Vivaldi antenna array.

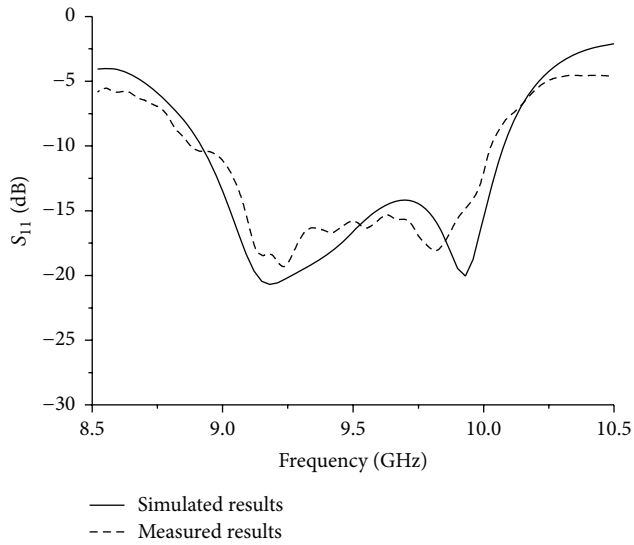

Figure 21: Reflection coefficient of the SIW Vivaldi antenna array.

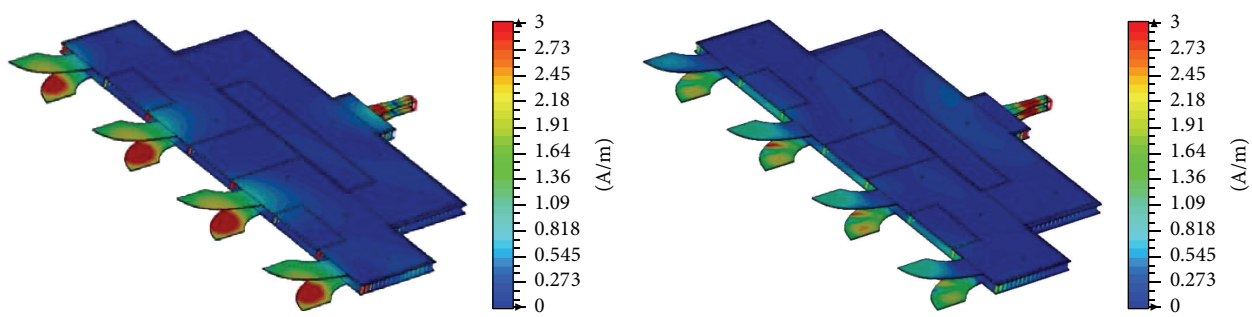

(a) Phase is 0 deg (b) Phase is 90 deg

Figure 22: Surface current of the SIW Vivaldi antenna array.

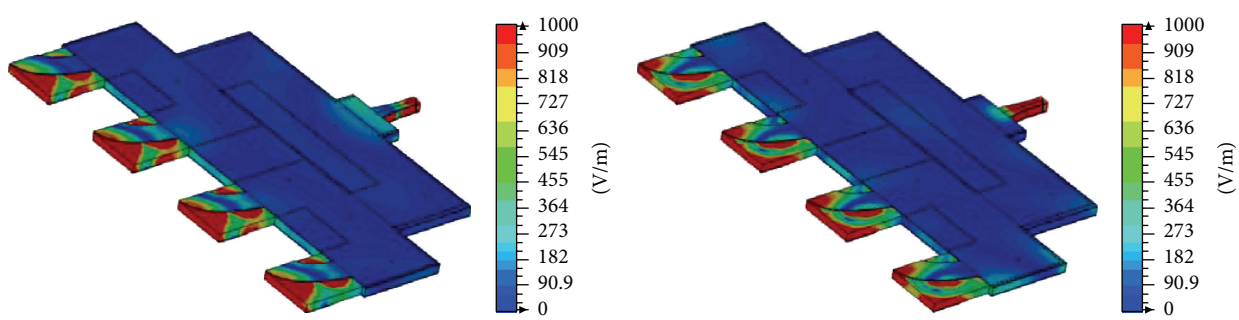

(a) Phase is 0 deg (b) Phase is 90 deg

Figure 23: Electric field of the SIW Vivaldi antenna array.

8.88 GHz to 10.02 GHz. The measurement shows agreement with the simulation.

The simulated surface current of the SIW Vivaldi antenna array on 9.5 GHz is shown in Figure 22. And the simulated electric field of the SIW Vivaldi antenna array on 9.5 GHz is shown in Figure 23.

The simulated and measured radiation patterns on 9.5 GHz of the SIW Vivaldi antenna array are shown in Figure 24. The array gain can reach 14 dB on 9.5 GHz in simulation, and the main lobe width is about 17.3°. The measured gain is about 13.3 dB, and the main lobe width is about 16.9°.

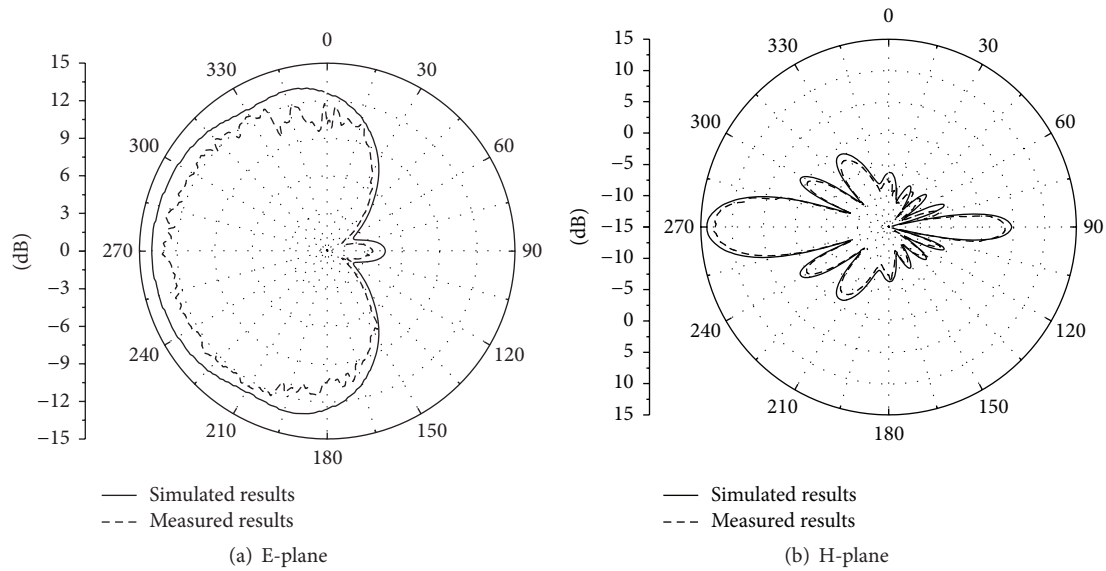

Figure 24: Pattern of the SIW Vivaldi antenna array on 9.5 GHz.

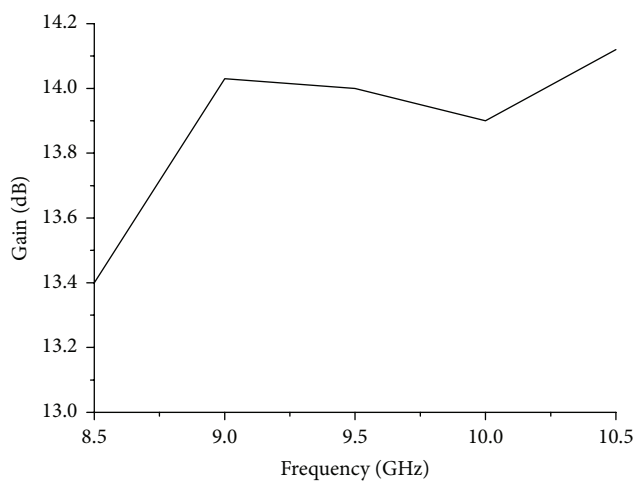

Figure 25: Simulated gain of the SIW Vivaldi antenna array.

Figure 25 is the simulated gain in operating band. It is shown that the gain is increased with frequency increasing.

4. Conclusion

A 4-way SIW equal power divider is designed, and the impedance characteristics and transmission characteristics satisfy the array design. The Vivaldi radiation element consisted of the antipodal structure. The operating bandwidth of the SIW Vivaldi array antenna is more than 1.1 GHz in X-band. And the gain of the array antenna is 13.3 dB on 9.5 GHz.

Conflict of Interests

The authors declare that there is no conflict of interests regarding the publication of this paper.

Acknowledgment

The authors would like to express their sincere gratitude to funds supported by "the National Natural Science Funds" (Grant no. 61501145).

References

[1] S. H. He, W. Shan, C. Fan, Z. C. Mo, F. H. Yang, and J. H. Chen, "An improved vivaldi antenna for vehicular wireless communication systems," *IEEE Antennas and Wireless Propagation Letters*, vol. 13, pp. 1505–1508, 2014.

[2] X. Zhuge and A. G. Yarovoy, "A sparse aperture MIMO-SAR-based UWB imaging system for concealed weapon detection," *IEEE Transactions on Geoscience and Remote Sensing*, vol. 49, no. 1, pp. 509–518, 2011.

[3] F. Fioranelli, S. Salous, I. Ndip, and X. Raimundo, "Through-the-wall detection with gated FMCW signals using optimized patch-like and Vivaldi antennas," *IEEE Transactions on Antennas and Propagation*, vol. 63, no. 3, pp. 1106–1117, 2015.

[4] J. D. S. Langley, P. S. Hall, and P. N. Newham, "Novel ultrawide-bandwidth Vivaldi antenna with low crosspolarisation," *Electronics Letters*, vol. 29, no. 23, pp. 2004–2005, 1993.

[5] R. Natarajan, J. V. George, M. Kanagasabai, and A. Kumar Shrivastav, "A compact antipodal Vivaldi antenna for UWB applications," *IEEE Antennas and Wireless Propagation Letters*, vol. 14, pp. 1557–1560, 2015.

[6] G. Teni, N. Zhang, J. Qiu, and P. Zhang, "Research on a novel miniaturized antipodal vivaldi antenna with improved radiation," *IEEE Antennas and Wireless Propagation Letters*, vol. 12, pp. 417–420, 2013.

[7] A. M. De Oliveira, M. B. Perotoni, S. T. Kofuji, and J. F. Justo, "A palm tree antipodal vivaldi antenna with exponential slot edge for improved radiation pattern," *IEEE Antennas and Wireless Propagation Letters*, vol. 14, pp. 1334–1337, 2015.

[8] S. Germain, D. Deslandes, and K. Wu, "Development of substrate integrated waveguide power dividers," in *Proceedings of the IEEE Canadian Conference on Electrical and Computer*

Engineering (CCECE '03), vol. 3, pp. 1921–1924, Montreal, Canada, May 2003.

[9] Z. Hao, W. Hong, H. Li, H. Zhang, and K. Wu, "Multiway broadband substrate integrated waveguide (SIW) power divider," in *Proceedings of the IEEE Antennas and Propagation Society International Symposium*, pp. 639–642, IEEE, July 2005.

[10] X. Zou, C.-M. Tong, and D.-W. Yu, "Y-junction power divider based on substrate integrated waveguide," *Electronics Letters*, vol. 47, no. 25, pp. 1375–1376, 2011.

[11] S. Yang, A. Elsherbini, S. Lin, A. E. Fathy, A. Kamel, and H. Elhennawy, "A highly efficient Vivaldi antenna array design on thick substrate and fed by SIW structure with integrated GCPW feed," in *Proceedings of the IEEE Antennas and Propagation Society International Symposium*, pp. 1985–1988, IEEE, Honolulu, Hawaii, USA, June 2007.

[12] L. Bin, D. Liang, and Z. Jiao-Cheng, "The research of broadband millimeter-wave Vivaldi array antenna using SIW technique," in *Proceedings of the International Conference on Microwave and Millimeter Wave Technology (ICMMT '10)*, pp. 997–1000, IEEE, Chengdu, China, May 2010.

[13] W. M. Abdel Wahab, D. Busuioc, and S. Safavi-Naeini, "Low cost planar waveguide technology-based dielectric resonator antenna (DRA) for millimeter-wave applications: analysis, design, and fabrication," *IEEE Transactions on Antennas and Propagation*, vol. 58, no. 8, pp. 2499–2507, 2010.

[14] L. Wang, X. Yin, and H. Zhao, "A planar feeding technology using phase-and-amplitude-corrected SIW horn and its application," *IEEE Antennas and Wireless Propagation Letters*, vol. 14, pp. 147–150, 2015.